

Supplemental material

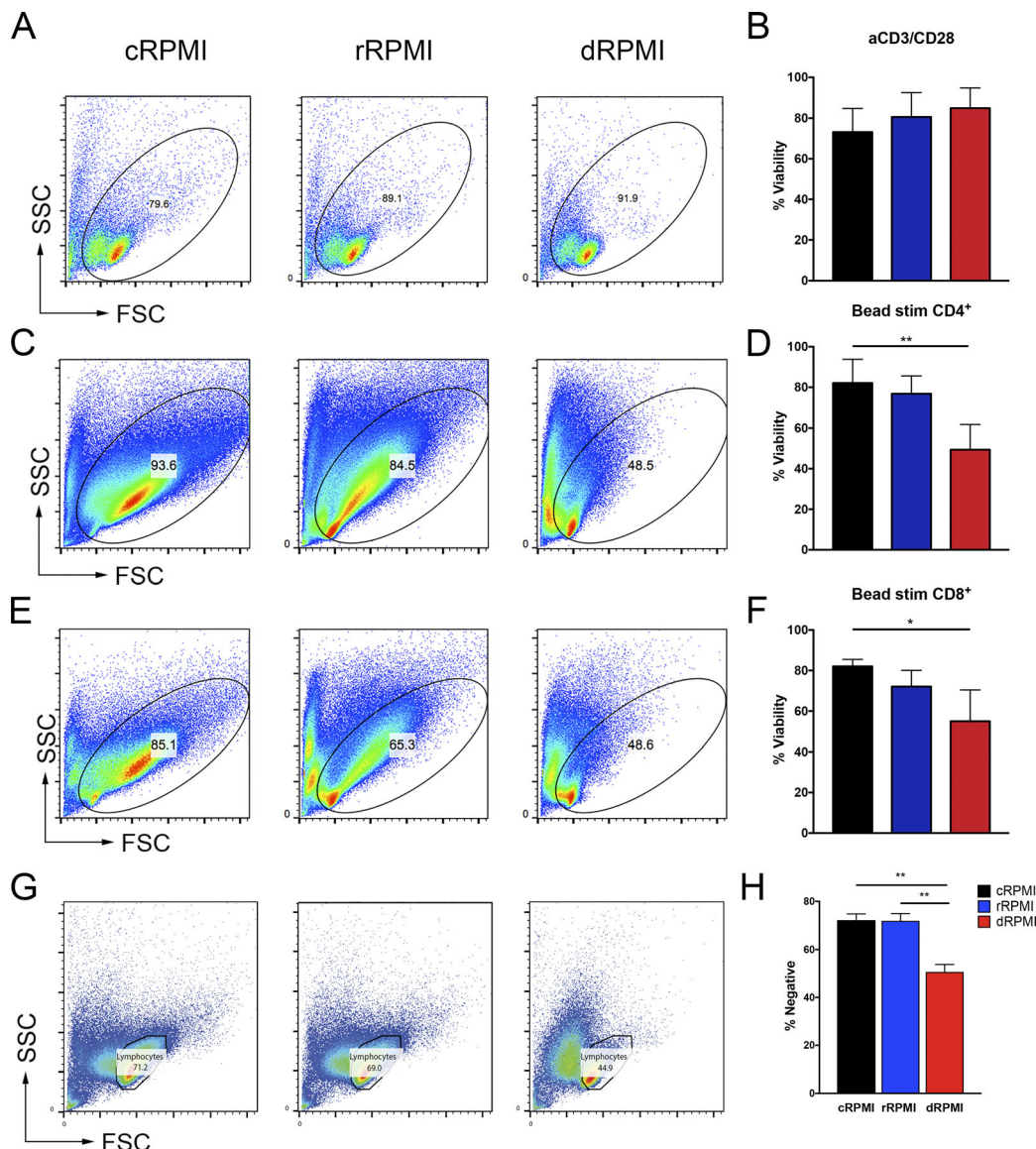
Kanellopoulou et al., <https://doi.org/10.1084/jem.20181970>

Figure S1. Cell viability of cells in media containing different concentrations of Mg²⁺. **(A)** Representative flow cytometric plots gated on live cell populations for each of the respective media conditions (cRPIMI, rRPIMI, and dRPIMI) used for experiments in Fig. 1, A and C. **(B)** Quantification of cell viability across all experimental repeats of Fig. 1, A and C. **(C and E)** Representative flow cytometric plots gated on live cell populations (CD4⁺ and CD8⁺, respectively) for each of the respective media conditions (cRPIMI, rRPIMI, and dRPIMI) used for experiments in Fig. 1 E. **(D and F)** Quantification of cell viability. Error bars represent mean and SEM from at least four independent experiments (A–H). **(G)** Representative flow plots of cell viability (Forward scatter [FSC] versus side scatter [SSC]) of cycling PBMCs cultured for 96 h in cRPIMI, rRPIMI, and dRPIMI. **(H)** Quantification of cell viability from eight independent experiments. P values were calculated using a paired t test (*, P < 0.05; **, P < 0.01).

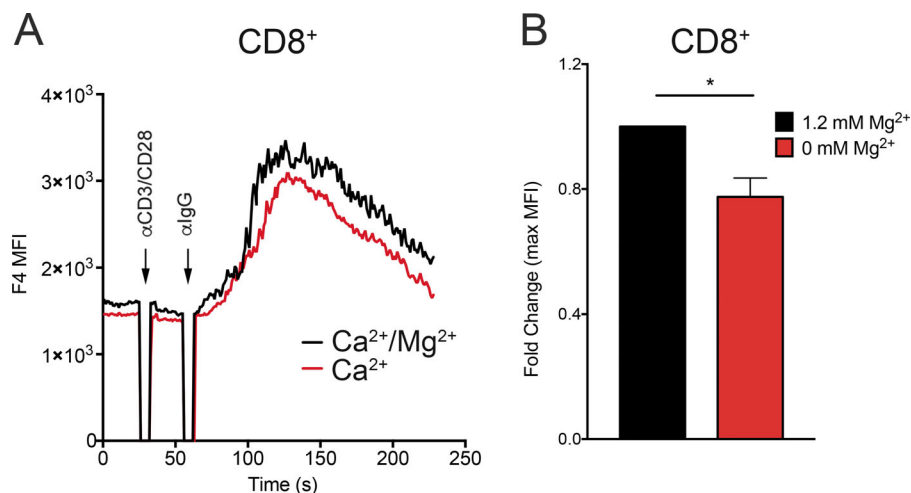


Figure S2. Acute Mg²⁺ deprivation impairs TCR signaling in CD8⁺ cells. (A) Flow cytometric analysis of Ca²⁺ flux plotted as MFI of Fluo-4 Ca²⁺ indicator versus time (s) in ex vivo-isolated PBMCs and CD8⁺ cells selected for analysis. Stimulation was performed in buffer containing only 1.2 mM CaCl₂ (Ca) or 1.2 mM CaCl₂ and 1.2 mM MgSO₄ (Ca²⁺/Mg²⁺). **(B)** Quantification of the fold change of the maximum mean fluorescence intensity (MFI) for A. Error bars represent the mean and SEM of four independent experiments. P values were calculated using a paired t test (*, P < 0.05; **, P < 0.01).

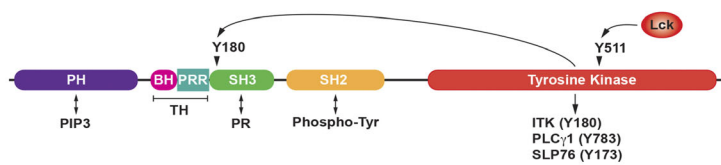
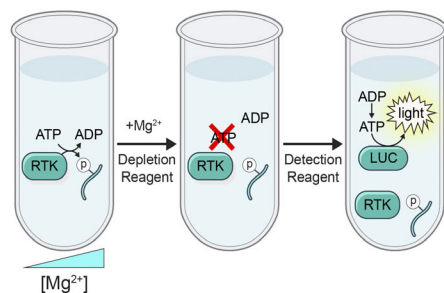
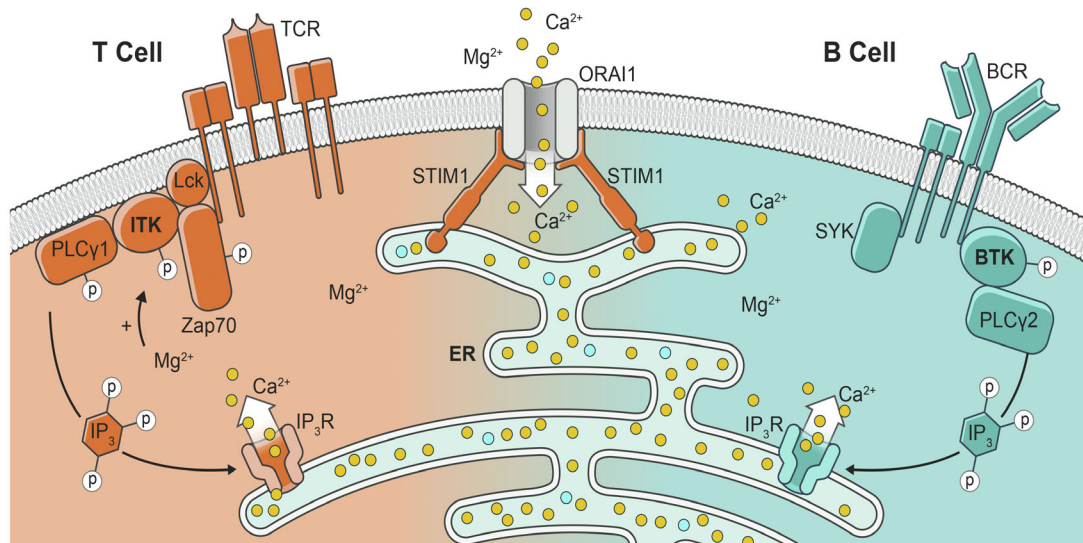
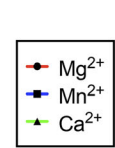
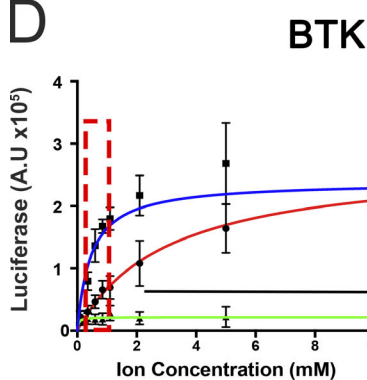
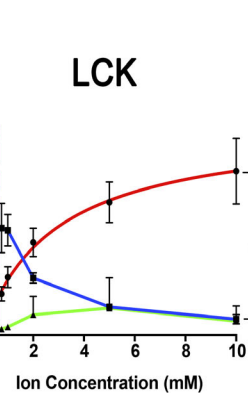
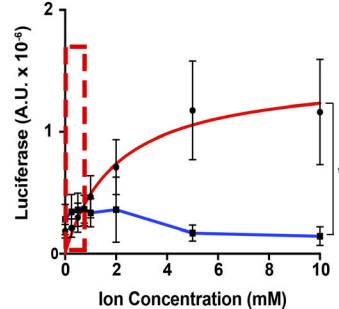
A**B****C****D****LCK****ZAP70**

Figure S3. Mg²⁺ promotes the activity of ITK and other immunologically relevant kinases. (A) Schematic of ITK protein domains: pleckstrin homology (PH), which binds phosphoinositol triphosphate (PIP₃); Tec homology (TH) domain containing a BTK homology (BH) and a proline-rich region (PR); src homology 3 (SH3), which binds proline-rich (PRR) polypeptides; src homology 2 (SH2), which binds phospho-Tyr residues (Tyr) residues; and the tyrosine kinase domain. The Lck substrate site (Y511) and autophosphorylation site (Y180) are indicated. Also shown are known ITK substrates. (B) Schematic of the luciferase (LUC)-based relevant tyrosine kinase (RTK) assay used to measure in vitro kinase activity. (C) Schematic of the TCR/BCR signaling pathways and the proposed regulatory role of Mg²⁺ during stimulation. (D) Kinase activity assay for BTK as a function of increasing MgCl₂ (red), MnCl₂ (blue), and CaCl₂ (green) concentrations. y axes represent luciferase activity (A.U.). Graph to the right shows an expanded axis containing the region boxed by the dashed black lines representing the approximate [Mg²⁺]_i measured in lymphocytes (Fig. 1 D). (E) Kinase activity assays for Lck (A) and ZAP70 (B) as a function of increasing millimolar concentrations of MgCl₂, MnCl₂, and CaCl₂. The regions boxed by the dashed red lines represent the approximate [Mg²⁺]_i measured in lymphocytes. y axes represent luciferase activity (A.U.). Data are the mean of three independent experiments \pm SEM (D and E). P values were calculated using a paired t test (*, P < 0.05; ** P < 0.01).

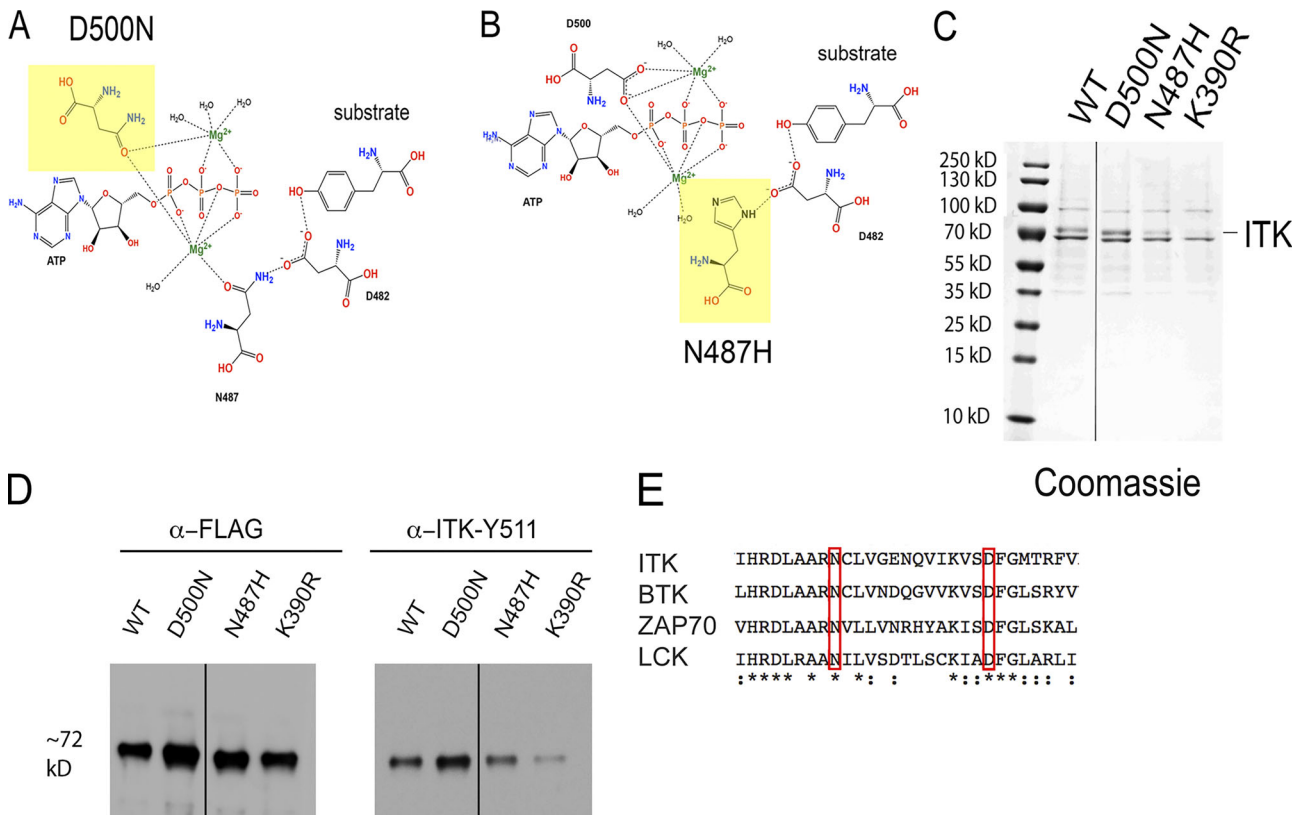


Figure S4. Purification of ITK mutant proteins. (A and B) Schematic representation of the ITK mutants D500N (A) and N487H (B) and their predicted effect on Mg²⁺ chelation. **(C)** Coomassie stain of FLAG-tagged ITK wild type and mutants after purification. **(D)** Western blot analysis of FLAG-tagged wild-type ITK protein and mutants purified from Expi293 cells with anti-FLAG and anti-ITK-Y511 antibodies as indicated. **(E)** Sequence alignment of other kinases involved in TCR signaling. The amino acids corresponding to D500 and N487 in ITK (red rectangles) are conserved in all kinases indicated.

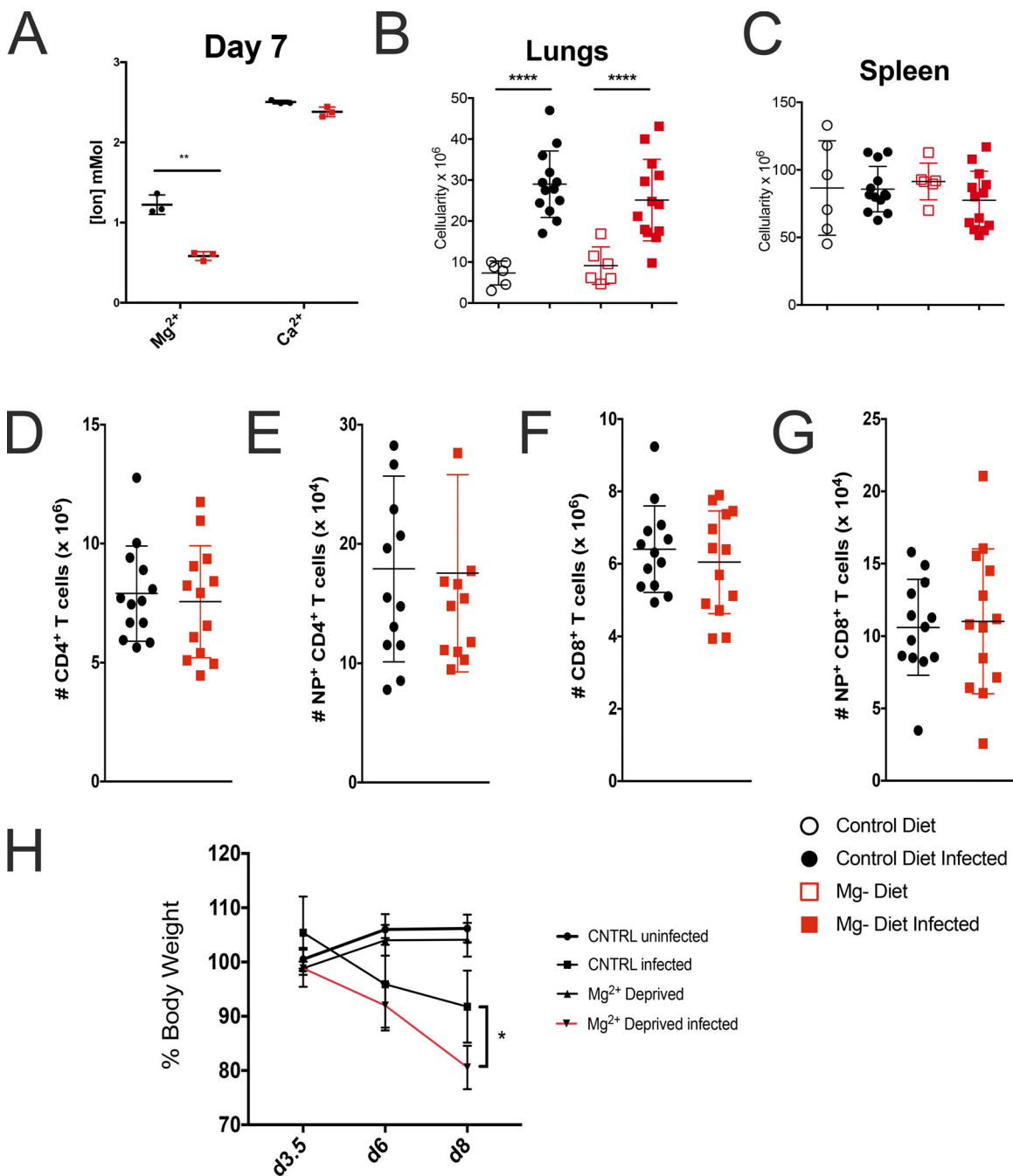


Figure S5. Mg²⁺ deprivation in mice decreases body weight but does not affect total lung cellularity and splenic T cells. (A) Representative Mg²⁺ serum levels at day 7 after mice (male C57BL/6) started a Mg²⁺-deficient diet. (B and C) Cell numbers from uninfected and infected mice from lungs (B) and spleen (C). (D–G) Quantification of the number of CD4⁺ (D), CD4⁺ NP tetramer⁺ (E), CD8⁺ (F), and CD8⁺ NP tetramer⁺ cells (G) in the spleen of control and Mg²⁺-deprived animals after flu infection. (H) Percent body weight of control and Mg²⁺-reduced diet (red) for A–G. Statistical significance was calculated with a Mann–Whitney U test (H) or an unpaired t test (G and N). *, P < 0.05; **, P < 0.01; ****, P < 0.0001.

Table S1. Parameters and constraints for the modified Hill equation

Parameter	Initial value	Rule	Constraint
φ	1	Value of Y at XMIN	>0
α	0	Initial value, to be fit	N/A
K_A	1	Value of X at YMID	>0
N	1	Initial value, to be fit	>0
R	Defined as the equilibrium ratio (Y parameter in Prism)		
t	Time (X parameter in Prism)		

Equilibrium values were obtained by calculating R (Y) when t (X) was set to 99,999 following the optimization of the above parameters. XMIN, minimum X value in dataset; YMID, middle Y value in dataset (average of minimum Y value and maximum Y value).

Table S2. Parameters and constraints for the Grynkiewicz model

Parameter	Initial value	Rule	Constraint
k	1	Initial value, to be fit	>0
R_{min}	1	*XMIN	>0
R_{max}	2	*XMIN	>0

R_{max} , ratio at 5 mM Mg²⁺; R_{min} , ratio at 0 mM Mg²⁺; XMIN, minimum X value in dataset.